

Simulations of liquid-crystal Fabry–Perot etalons by an improved 4×4 matrix method

Yuhua Huang

School of Optics/CREOL, University of Central Florida, Orlando, Florida 32816-2700

Thomas X. Wu

School of EE & CS, University of Central Florida, Orlando, Florida 32816

Shin-Tson Wu^{a)}

School of Optics/CREOL, University of Central Florida, Orlando, Florida 32816-2700

(Received 4 October 2002; accepted 5 December 2002)

The optical performances of a liquid crystal (LC) Fabry–Perot (FP) etalon in various configurations were simulated by a faster 4×4 matrix method. Results show that the FP with a 90° twisted nematic LC is polarization insensitive if the applied voltage exceeds ~3X of the Freedericksz transition threshold. This method can well depict the transmission spectra of the FP cavity and, therefore, is useful for optimizing the FP tunable filters for telecommunications. © 2003 American Institute of Physics. [DOI: 10.1063/1.1542652]

I. INTRODUCTION

Wavelength-tuning devices are commonly used in spectroscopy and high-density wavelength-division multiplexing system. Gratings and prisms are rather bulky even though they can perform wavelength selection remarkably well. An electrically tunable liquid crystal (LC) Fabry–Perot (FP) filter is an attractive wavelength-tuning device which allows for high finesse, low-power consumption, and compactness. In such a FP structure, LC is used as an active medium and the wavelength-tuning property is determined by the voltage-dependent LC phase as well as the alignment geometry.^{1–3} LC-based FP tunable filters have been experimentally investigated in different configurations. The optical behavior of LC FP cavity has not been theoretically analyzed in detail.

The Jones matrix⁴ and the 4×4 matrix^{5–7} methods are most frequently used to represent the electro-optical properties of LC devices. However, the Jones matrix method is not appropriate to represent the FP effect because it neglects the boundary conditions. On the other hand, the 4×4 matrix method does include the boundary condition and, thus, it is a good method for investigating the FP effect. The 4×4 matrix method was introduced by Teitler and Hennis⁵ and later applied to liquid crystal devices by Berreman.⁶ The key to this method is to find a 4×4 transfer matrix relating the tangential components of the electric and magnetic fields at the entrance of a device to those at the exit. In an inhomogeneous optical medium, however, an analytical expression for the 4×4 matrix does not exist. In this case, the inhomogeneous medium has to be divided into many slices with each regarded as homogeneous. The thickness of each slice must satisfy the condition that the thickness multiplied by the wave vector of the light is much smaller than a unit. A general problem of this approach is that the required numerical calculation time is quite long.

In this article, we derived the 4×4 matrix starting from Maxwell's equations through a different way from Berreman⁶ and Wöhler.⁷ In our derivation, the 4×4 matrix for each slice was diagonalized, thus the equations became very concise. We finally transferred the 4×4 matrix to scattering matrix. With the 4×4 matrix as well as scattering matrix method, we investigated the optical performance of nematic LC FP cavity in various configurations. The simulation results are in good agreement with the reported experimental results. The method is then applied to design the LC FP filters.

II. FASTER 4×4 MATRIX METHOD

Generally, a monochromatic plane wave consists of both electric [$\mathbf{E}(\mathbf{r},t)$] and magnetic [$\mathbf{H}(\mathbf{r},t)$] field, which can be written as $\mathbf{E}(\mathbf{r},t) = \mathbf{E}(\mathbf{r})\exp(j\omega t)$ and $\mathbf{H}(\mathbf{r},t) = \mathbf{H}(\mathbf{r})\exp(j\omega t)$. Therefore, for the medium without free charge and current, Maxwell's equations in the Gaussian units have following forms:

$$\nabla \times \mathbf{E} = -j\omega \mathbf{B}, \quad (1)$$

$$\nabla \cdot \mathbf{D} = 0, \quad (2)$$

$$\nabla \times \mathbf{H} = j\omega \mathbf{D}, \quad (3)$$

$$\nabla \cdot \mathbf{B} = 0, \quad (4)$$

where

$$\mathbf{B} = \mu_0 \mu \mathbf{H}, \quad (5)$$

$$\mathbf{D} = \epsilon_0 \epsilon_r \mathbf{E} = \epsilon_0 \begin{bmatrix} \epsilon_{xx} & \epsilon_{xy} & \epsilon_{xz} \\ \epsilon_{yx} & \epsilon_{yy} & \epsilon_{yz} \\ \epsilon_{zx} & \epsilon_{zy} & \epsilon_{zz} \end{bmatrix} \mathbf{E}, \quad (6)$$

μ is the magnetic tensor. For liquid crystals, we can assume $\mu \sim 1$. ϵ_r is the dielectric tensor, and

$$\epsilon_{xx} = n_o^2 + (n_e^2 - n_o^2) \cos^2 \theta \cos^2 \phi, \quad (7)$$

^{a)}Electronic mail: swu@mail.ucf.edu

$$\epsilon_{xy} = \epsilon_{yx} = (n_e^2 - n_o^2) \cos^2 \theta \sin \phi \cos \phi, \tag{8}$$

$$\epsilon_{xz} = \epsilon_{zx} = (n_e^2 - n_o^2) \sin \theta \cos \theta \cos \phi, \tag{9}$$

$$\epsilon_{yy} = n_o^2 + (n_e^2 - n_o^2) \cos^2 \theta \sin^2 \phi, \tag{10}$$

$$\epsilon_{yz} = \epsilon_{zy} = (n_e^2 - n_o^2) \sin \theta \cos \theta \sin \phi, \tag{11}$$

$$\epsilon_{zz} = n_o^2 + (n_e^2 - n_o^2) \sin^2 \theta \tag{12}$$

where n_o and n_e are the ordinary and extraordinary refractive indices of the LC, respectively. For an arbitrary orthogonal xyz coordinate system, θ is the angle between the LC director and the z axis and ϕ is the angle between the projection of the LC director on the x - y plane and the x axis.

For mathematical simplicity, magnetic field can be normalized by

$$\hat{\mathbf{H}} = \eta_0 \mathbf{H} = \sqrt{\frac{\mu_0}{\epsilon_0}} \mathbf{H}. \tag{13}$$

We will now consider a plane wave incident at oblique angle on the surface of a LC FP device as shown in Fig. 1. Without losing the generality, we can always choose an xyz coordinate system to ensure the incident wave vector \mathbf{k} lies on the x - z plane, the x - y plane parallel to the surface of FP and the direction of the $+z$ axis normal to the surface of FP cavity. Thus we have

$$\begin{aligned} \frac{\partial}{\partial y} &= 0 \\ \frac{\partial}{\partial x} &= -jk_x = -jk_0 \sin \theta, \end{aligned} \tag{14}$$

where $k_0 = \omega \sqrt{\mu_0 \epsilon_0} = 2\pi/(\lambda) \sqrt{\mu_0 \epsilon_0}$, λ is the wavelength of incident light in free space.

Substituting Eqs. (13) and (14) into Eqs. (1) and (3), we can finally get the following equation after mathematical derivation:

$$Q = \begin{bmatrix} -\frac{\epsilon_{zx}}{\epsilon_{zz}} \sin(\theta) & 1 - \frac{\sin^2(\theta)}{\epsilon_{zz}} & -\frac{\epsilon_{zy}}{\epsilon_{zz}} \sin(\theta) & 0 \\ \epsilon_{xx} - \frac{\epsilon_{zx}}{\epsilon_{zz}} \epsilon_{zx} & \frac{-\sin(\theta)}{\epsilon_{zz}} \epsilon_{xz} & \epsilon_{xy} - \frac{\epsilon_{zy}}{\epsilon_{zz}} \epsilon_{zy} & 0 \\ 0 & 0 & 0 & 1 \\ \epsilon_{yx} - \frac{\epsilon_{zx}}{\epsilon_{zz}} \epsilon_{yx} & -\frac{\epsilon_{yz}}{\epsilon_{zz}} \sin(\theta) & \epsilon_{yy} - \frac{\epsilon_{zy}}{\epsilon_{zz}} \sin^2(\theta) & 0 \end{bmatrix}. \tag{16}$$

When Q is not a function of z , it can be diagonalized as:

$$Q = T \begin{bmatrix} q_1 & & & \\ & q_2 & & \\ & & -q_3 & \\ & & & -q_4 \end{bmatrix} T^{-1}. \tag{17}$$

This is available for each layer even in an inhomogeneous cell if we divide the cell into many layers to ensure that each layer can be regarded as homogeneous. In this article, we

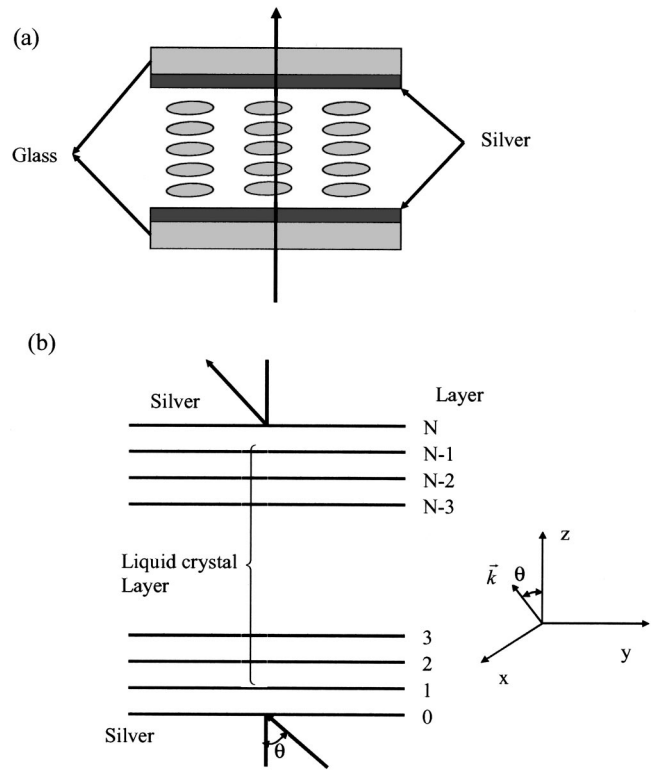


FIG. 1. Schematic diagram of a LC Fabry-Perot cavity divided into N layers. The propagation vector \mathbf{k} lies in the x - z plane.

$$\frac{\partial}{\partial z} \begin{bmatrix} E_x \\ \hat{H}_y \\ E_y \\ -\hat{H}_x \end{bmatrix} = -jk_0 Q \begin{bmatrix} E_x \\ \hat{H}_y \\ E_y \\ -\hat{H}_x \end{bmatrix}, \tag{15}$$

where

used the diagonalized 4×4 matrix to represent the optical behavior of each layer. This makes the derivation more straightforward and equations more concise than those developed by Berreman⁶ and Wöhler⁷.

For normal incidence, it is much faster to use an extended Jones matrix method⁸ than the 4×4 matrix method if multiple interferences are neglected. For display cells, the extended Jones matrix has been used widely. However, interference effect dominates in the Fabry-Perot cavity and we have to use the 4×4 matrix method.

As illustrated in Fig. 1, the entire LC FP system is divided into N layers. The first and last layers are reflective dielectrics such as silver. The LC layer is divided into $N-2$ sublayers with each layer characterized by a corresponding dielectric tensor. From Eq. (15), we can obtain the electric and magnetic field components $E_x, \hat{H}_y, E_y, \hat{H}_x$ at exit as the function of those at entrance

$$\begin{bmatrix} E_x \\ \hat{H}_y \\ E_y \\ -\hat{H}_x \end{bmatrix}_N = P \begin{bmatrix} E_x \\ \hat{H}_y \\ E_y \\ -\hat{H}_x \end{bmatrix}_0, \tag{18}$$

where

$$P = P_N P_{N-1} \dots P_1, \tag{19}$$

and

$$P_n = T_n \begin{bmatrix} (-jk_0 q_1 \Delta z) & & & \\ & (-jk_0 q_2 \Delta z) & & \\ & & (-jk_0 q_3 \Delta z) & \\ & & & (-jk_0 q_4 \Delta z) \end{bmatrix} T_n^{-1}, \tag{20}$$

and $n=1,2,\dots,N$. Equation (20) is the 4×4 matrix representation at the oblique incidence for each layer.

In the above derivation, we just considered the waves propagating towards $+z$ direction. In fact, there are always four eigenwaves propagating in the opposite direction in each layer of the FP cell. The two eigenwaves propagating towards the $+z$ direction are transmitted waves, and the remaining two propagating towards the $-z$ direction are reflected waves. In the same medium, the amplitudes of reflected waves are generally much smaller than those of the transmitted waves, therefore can be neglected but they cannot be neglected at the entrance and exit because of the large reflectivity mirrors. Considering the propagation of both reflected and transmitted waves and using the boundary condition, we get the four eigenwaves at the exit which relate to the four eigenwaves at the entrance as

$$\begin{bmatrix} E_{xN}^+ \\ E_{yN}^+ \\ E_{xN}^- \\ E_{yN}^- \end{bmatrix}_N = N \begin{bmatrix} E_{x0}^+ \\ E_{y0}^+ \\ E_{x0}^- \\ E_{y0}^- \end{bmatrix}_0, \tag{21}$$

where

$$N = T_{N+1}^{-1} P T_0, \tag{22}$$

and

$$T_0 = \begin{bmatrix} 1 & 0 & 1 & 0 \\ \frac{\epsilon_r}{\sqrt{\epsilon_{rz}}} & 0 & -\frac{\epsilon_r}{\sqrt{\epsilon_{rz}}} & 0 \\ 0 & 1 & 0 & 1 \\ 0 & \sqrt{\epsilon_{rz}} & 0 & -\sqrt{\epsilon_{rz}} \end{bmatrix}, \tag{23}$$

$$T_{N+1}^{-1} = \begin{bmatrix} \frac{1}{2} & \frac{\sqrt{\epsilon_{rz}}}{2\epsilon_r} & 0 & 0 \\ 0 & 0 & \frac{1}{2} & \frac{1}{2\sqrt{\epsilon_{rz}}} \\ \frac{1}{2} & -\frac{\sqrt{\epsilon_{rz}}}{2\epsilon_r} & 0 & 0 \\ 0 & 0 & \frac{1}{2} & -\frac{1}{2\sqrt{\epsilon_{rz}}} \end{bmatrix}, \tag{24}$$

T_0 and T_{N+1} are the eigenmatrices at entrance and exit, respectively. In order to simplify the calculation, we transfer the 4×4 matrix to a scattering matrix. Defining

$$N_{11} = \begin{bmatrix} n_{11} & n_{12} \\ n_{21} & n_{22} \end{bmatrix}, \quad N_{12} = \begin{bmatrix} n_{13} & n_{14} \\ n_{23} & n_{24} \end{bmatrix},$$

$$N_{21} = \begin{bmatrix} n_{31} & n_{32} \\ n_{41} & n_{42} \end{bmatrix}, \quad N_{22} = \begin{bmatrix} n_{33} & n_{34} \\ n_{43} & n_{44} \end{bmatrix},$$

and $E_j = \begin{bmatrix} E_{xj} \\ E_{yj} \end{bmatrix}$, Eq. (21) can be rewritten as

$$\begin{bmatrix} E_N^+ \\ E_N^- \end{bmatrix} = \begin{bmatrix} N_{11} & N_{12} \\ N_{21} & N_{22} \end{bmatrix} \begin{bmatrix} E_0^+ \\ E_0^- \end{bmatrix}. \tag{25}$$

After some mathematics, we derive the reflected waves at the entrance and the transmitted waves at the exit as

$$\begin{bmatrix} E_0^- \\ E_N^+ \end{bmatrix} = \begin{bmatrix} S_{11} & S_{12} \\ S_{21} & S_{22} \end{bmatrix} \begin{bmatrix} E_0^+ \\ E_N^- \end{bmatrix}, \tag{26}$$

where $S_{12} = N_{22}^{-1}$, $S_{11} = -S_{12} N_{21}$, $S_{21} = N_{11} + N_{12} S_{11}$, $S_{22} = N_{12} S_{12}$. For the transmission mode, $E_N^- = 0$ so we can get

$$E_N^+ = S_{21} E_0^+. \tag{27}$$

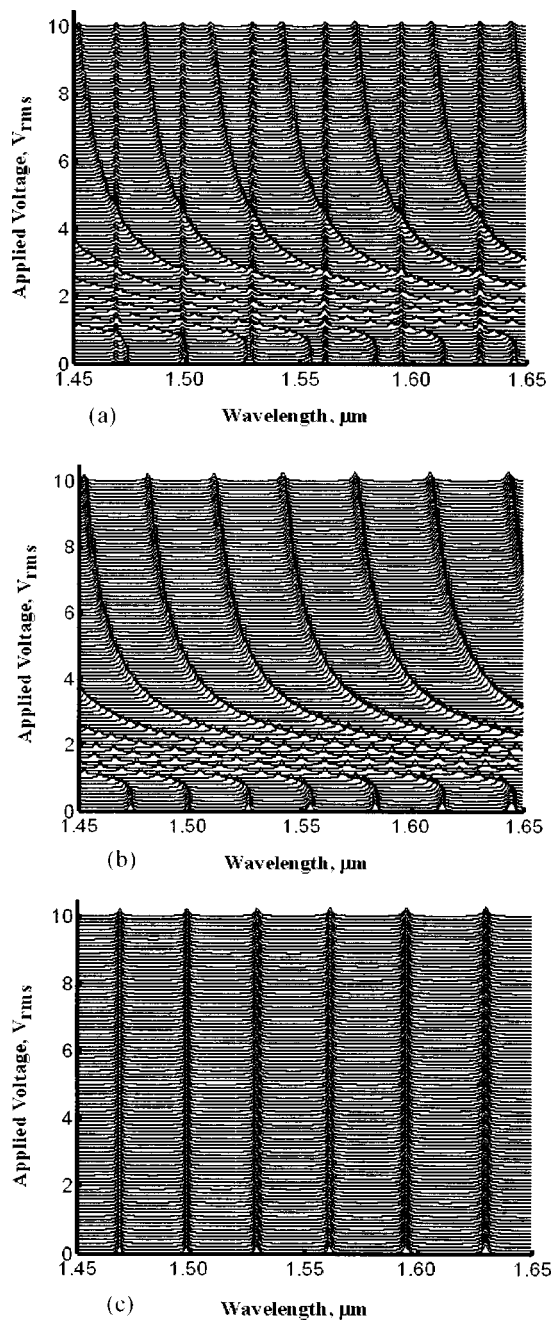


FIG. 2. Voltage-dependent transmittance of a homogeneous cell in a Fabry-Perot cavity: (a) unpolarized light; (b) e ray, and (c) o ray; $d=25 \mu\text{m}$ and the LC of E7 was used.

III. RESULTS AND DISCUSSIONS

We developed a program to simulate the transmission spectra of the LC FP cavity. A commercial nematic E7 LC mixture (from Merck) was used as an example. The material parameters of E7 are $n_o=1.5$, $n_e=1.713$, the dielectric anisotropy $\Delta\epsilon=14.3$, the splay elastic constant $k_{11}=11.7 \times 10^{-12}\text{N}$, twist elastic constant $k_{22}=9.0 \times 10^{-12}\text{N}$, and bend elastic constant $k_{33}=19.5 \times 10^{-12}\text{N}$. Silver with refractive index $n=0.2+i3.44$ was used as reflectors for the FP cavity. Two LC cells are studied: homogeneous and 90° twisted-nematic (TN) cells. In a homogeneous cell, the front and rear LC directors are parallel to each other and in a

90° -TN cell the rear LC director is twisted 90° from the front.⁹ The electric field is applied in the longitudinal direction. Our simulation results agree very well with those obtained from Jones matrix and Berreman's 4×4 matrix methods, except for a faster calculation time.

A. Homogeneous LC cell

Figure 2 shows the simulated transmission spectra of the unpolarized and linearly polarized input beams through a homogeneous LC FP cell at various voltages. The spectral range considered is from $\lambda=1.45$ to $1.65 \mu\text{m}$ for telecommunication applications. Figure 2(a) shows the results for the unpolarized light. There are always two modes propagating in the FP cavity at various voltages. The vertical pulse trains represent the ordinary optical mode with n_o which is independent of the applied voltage. The other pulse train whose transmission shifts toward the shorter wavelength side as the applied voltage increases is attributed to the extraordinary optical mode with n_e . As the voltage increases, the n_e of the LC decreases rather quickly in the beginning and then gradually saturates. As a result, the corresponding wavelength rapidly shifts to a shorter wavelength as the voltage increases. Beyond $3-4 V_{\text{rms}}$, the wavelength shift gradually saturates. It takes a relatively large voltage swing to change the peak transmission wavelength. These simulation results are in good agreement with those reported previously.¹

Figures 2(b) and 2(c) show the results for the extraordinary and ordinary rays, respectively. Here, the ordinary ray (o mode) refers to that the incident linear polarization is perpendicular to the LC director and the extraordinary ray (e mode) is parallel. The transmission of the circularly polarized light is the same as that of the unpolarized light, as shown in Fig. 2(a). A circularly polarized light can also be decomposed into two orthogonal linear polarizations, thus, the results are superposition of Figs. 2(b) and 2(c). In either case, the LC FP in the homogeneous cell is polarization sensitive.

B. 90° -TN cell

Figures 3(a)–3(c) depict the voltage-dependent transmittance of the 90° twist nematic LC in the FP cavity for the unpolarized and linearly (e and o ray) polarized incident light, respectively. Results are quite intriguing. The Freedericksz threshold voltage¹⁰ is defined as:

$$V_{th} = \pi \sqrt{\frac{K_{11} + (K_{33} - 2K_{22})/4}{\epsilon_0 \Delta\epsilon}}. \tag{28}$$

For an E-7 TN cell, V_{th} is $\sim 0.96 V_{\text{rms}}$. However, in a TN cell, another optical threshold¹¹ exists where the polarization rotation effect is disrupted. For E-7, the optical threshold is $V_{op} \sim 2.0 V_{\text{rms}}$ (or $V_{op} \sim 2 V_{th}$). Below V_{th} , the FP transmittance depends on the input polarization. For a linearly polarized light, there is only one mode (either ordinary or extraordinary) propagating in the cavity. While for an unpolarized or a circularly polarized beam, both o and e mode exist in the FP cavity. In this regime, the Mauguin condition for the polarization rotation effect holds so that the two modes are decoupled.

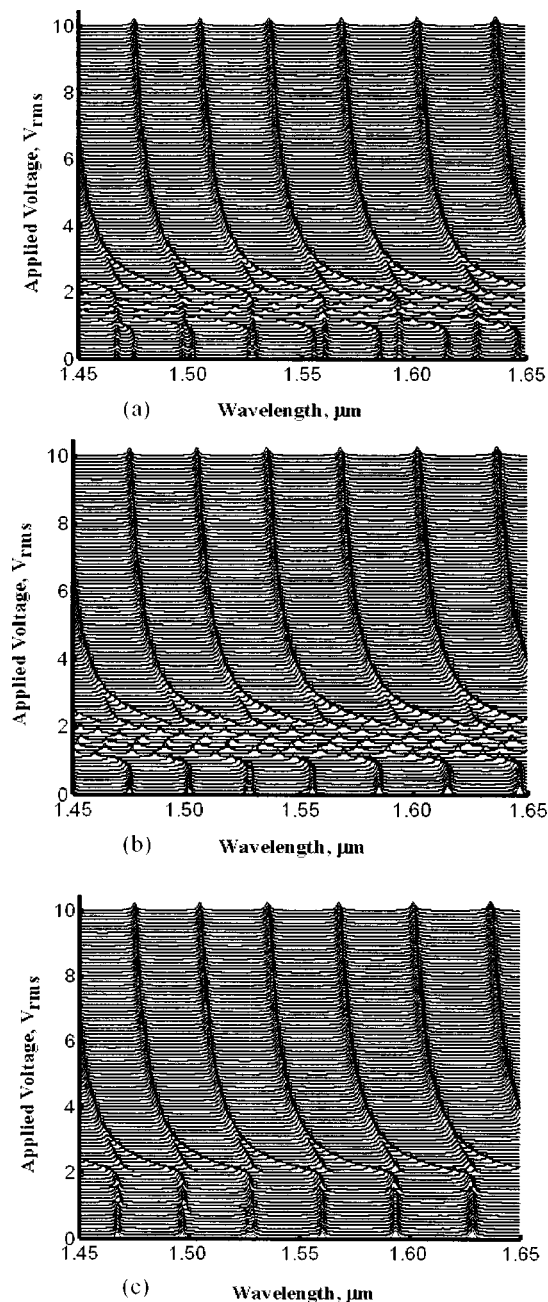


FIG. 3. Voltage-dependent transmittance of a 90°-TN cell in a Fabry-Perot cavity: (a) unpolarized light; (b) e ray, and (c) o ray; $d = 25 \mu\text{m}$ and the LC of E7 was used.

In the $V_{th} < V < V_{op}$ regime, the LC directors start to tilt while retaining the uniform twist. Such molecular tilt decreases the effective birefringence of the LC layer and rapidly shifts the e mode toward the short wavelength side, as observed in Fig. 3(b). On the other hand, such molecular tilt does not affect the o-mode propagation.¹² Figure 3(c) shows that the o mode is affected only when $V > V_{op}$ regime. That is to say, the e mode responds to the Fredericksz transition threshold whereas the o mode follows the optical threshold.

In the $2 < V < 3 V_{rms}$ (or $2 < V/V_{th} < 3$), the twist in the LC bulk is broken so that the Mauguin condition is no longer satisfied. Mode mixing occurs so that the eigenmodes in the cavity are no longer linearly polarized along or perpendicular

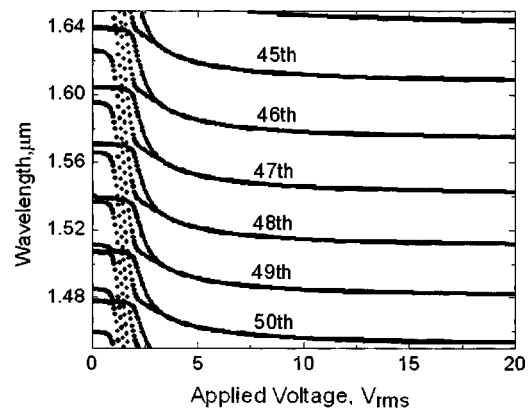


FIG. 4. Mode propagation of a Fabry-Perot tunable filter using 90°-TN cell: $d = 25 \mu\text{m}$ and the LC of E7 was used. The incident light is unpolarized. At $V = 0$, o and e modes are separated. The peaks of the 45–50th modes are at 1.67, 1.63, 1.59, 1.565, 1.53, and 1.5 μm for o ray, and at 1.90, 1.86, 1.82, 1.78, 1.74, and 1.71 μm for e ray, respectively. At $V > 3 V_{rms}$, the TN cell is independent of polarization and the same modes of o and e ray merge into one.

to the LC directors. Under such a circumstance, the TN LC cell has elliptical polarization state. The elliptical polarization can be decomposed into two orthogonal linear polarizations such as the e and o mode, corresponding to the two separated peaks, as shown in Figs. 3(b) and 3(c).

In the $V > 3 V_{rms}$ (or $V/V_{th} > 3$) regime, the e and o mode merge together as shown in Figs. 3(a)–3(c). This indicates such a voltage-biased 90°-TN cell is independent of polarization. In a 90°-TN cell, the two boundary layers are orthogonal. At $V > 3 V_{th}$, the bulk LC directors are reoriented perpendicular to the substrates by the electric field. The phase retardation of the two boundary layers compensates each other. If the incoming linearly polarized light is an e ray to the front surface, it will behave like an o ray to the rear surface, and vice versa. As a result, the LC cell is independent of polarization. This quantitative result was observed by Patel in his experimental studies.³ Our 4×4 matrix analyses confirm this important experimental observation. Therefore, the TN cell has isotropic, yet tunable refractive index in the $V > 3 V_{th}$ regime. New applications of using 90°-TN cell for polarization-independent phase modulators could be realized.

As the applied voltage exceeds $3 V_{th}$, the LC directors continue to tilt leading to a decreased refractive index. To evaluate the available residual phase, we use our modified 4×4 matrix method to calculate the wavelength shift in the 3–20 V_{rms} region. Through this wavelength shift, the change of refractive index can be extracted.

Figure 4 shows the mode propagation for an unpolarized light in a 90° twisted nematic LC FP cell. Thirteen transmission peaks appear within the 1.45–1.65 μm wavelength range at $V = 0$, which relate to different o and e modes, respectively. The m th mode can be obtained from the following equation:

$$2nd = m\lambda. \quad (29)$$

In Eq. (29), n is the refractive index, d is the cell gap, λ is the wavelength, and m is the order of the mode propagating in

the FP cavity. In our simulation, we used a $d=25\ \mu\text{m}$ E7 Fabry–Perot cell. Using Eq. (2), we can easily get the 45th–50th mode within the 1.45–1.65 μm wavelength range as labeled in Fig. 4. Here we used the 48th transmission mode as an example to illustrate the voltage-dependent optical characteristics of the 90°-TN FP tunable filter. Below Freedericksz transition threshold, the peaks of the 48th ordinary and extraordinary modes are separated, at ~ 1.57 and $\sim 1.78\ \mu\text{m}$, respectively. The two peaks begin to merge into one when the applied voltages exceed $\sim 3 V_{\text{rms}}$. This indicates that the effective birefringence of the TN cell is zero in this regime.

In Fig. 4, the remaining effective refractive index of the TN cell is calculated to be about 0.02 (or 10% of the LC birefringence) when the applied voltage is increased from 3 to $20 V_{\text{rms}}$. To obtain a larger refractive index change, high birefringence liquid crystals are more favorable.¹³

Figures 2 and 3 show that the LC twisted angle makes a large effect on the transmission characteristics of a FP etalon. In the $V > 3 V_{th}$ regime, the FP with 90° twisted nematic LC cell is polarization insensitive at normal incidence. Actually, other parameters including cell gap, refractive index and thickness of the reflector, and the incident direction can also affect the transmission characteristics. A thinner cell gap compresses the number of transmission modes and widens the wavelength tunable range and the linewidth of each mode. The reflectivity, refractive index, and thickness of the reflector in the FP cavity also affect the wavelength tunable range, linewidth, and peak of transmission. Choosing a set of suitable parameters is essential for optimizing the performance of the FP cavity. These can be done with the program based on the 4×4 matrix methods.

IV. CONCLUSIONS

The transmission performances of LC FP cavity in various configurations were investigated with the faster 4×4 matrix method. The simulation results with this method are in good agreement with the previously published experimental results. At normal incidence, the Fabry–Perot tunable filter based on the 90° twisted nematic LC is polarization insensitive when $V > 3 V_{th}$. The modified 4×4 matrix method we present here can depict the transmission performance of the FP cavity and, therefore, can be used for optimizing the FP tunable filters for telecom applications.

ACKNOWLEDGMENTS

The authors would like to thank Dr. Xinyu Zhu, School of Optics at UCF, for useful discussions. This work is supported by DARPA under Contract No. DAAD19-02-1-0208.

- ¹J. H. Lee, H. R. Kim, and S. D. Lee, *Appl. Phys. Lett.* **75**, 859 (1999).
- ²J. S. Patel and S. D. Lee, *Appl. Phys. Lett.* **58**, 2491 (1991).
- ³J. S. Patel, *Appl. Phys. Lett.* **58**, 1314 (1991).
- ⁴R. C. Jones, *J. Opt. Soc. Am. A* **31**, 488 (1941).
- ⁵S. Teitler and B. Hennis, *J. Opt. Soc. Am.* **60**, 830 (1970).
- ⁶D. W. Berreman, *J. Opt. Soc. Am.* **62**, 502 (1972); **63**, 1374 (1973).
- ⁷H. Whöler, G. Haas, M. Fritsch, and D. A. Mlynski, *J. Opt. Soc. Am. A* **5**, 1554 (1988).
- ⁸A. Lien, *Liq. Cryst.* **22**, 171 (1997).
- ⁹M. Schadt and W. Helfrich, *Appl. Phys. Lett.* **18**, 127 (1971).
- ¹⁰V. Freedericksz and V. Zolina, *Trans. Faraday Soc.* **29**, 919 (1933).
- ¹¹D. W. Berreman, *Appl. Phys. Lett.* **25**, 12 (1974).
- ¹²N. Konforti, E. Maron, and S. T. Wu, *Opt. Lett.* **13**, 251 (1988).
- ¹³S. T. Wu and D. K. Yang, *Reflective Liquid Crystal Displays* (Wiley, New York, 2001).